

1.1 The Advanced Superconducting Test Accelerator (ASTA) at Fermilab [<http://asta.fnal.gov>]

Elvin Harms, Jerry Leibfritz, Sergei Nagaitsev, Philippe Piot^{*}, Jinhao Ruan,
Vladimir Shiltsev, Giulio Stancari, Alexander Valishev
Mail to: piot@fnal.gov
Fermi National Accelerator Laboratory, Batavia IL 60510

1.1.1 Introduction

The Advanced Superconducting Test Accelerator (ASTA) facility currently under construction and commissioning at Fermilab will enable a broad range of beam-based experiments to study fundamental limitations to beam intensity and to develop transformative approaches to particle-beam generation, acceleration and manipulation [1]. Three main elements of the ASTA facility include the Integrable Optics Test Accelerator (IOTA) ring capable of storing electrons or protons; b) 150-300 MeV electron injector based on existing ASTA SRF electron linac; c) 2.5 MeV proton injector based on existing HINS proton source. ASTA is intended to be operated as a test facility for advanced accelerator research and developments (AARD) towards intensity frontier proton accelerators. It is anticipated that experimental studies at ASTA's IOTA ring with protons and electrons, augmented with corresponding modelling and design efforts should pave the way for a proposal that will allow substantial increase of the proton flux available for high-energy Physics research with Fermilab accelerators at a lower cost. ASTA will be the only accelerator R&D facility in the worldwide. ASTA will support the development of new ideas towards the next generation high-intensity proton facilities and allows a broad range of intensity-frontier-motivated experiments, such as *integrable optics* with non-linear magnets and with electron lenses, and *space-charge compensation* with electron lenses and electron columns.

At the same time, ASTA will establish a unique resource for R&D towards Energy-Frontier facilities and a test-bed for SRF accelerators and high-brightness-beam applications. The unique features of ASTA include: (1) a high repetition-rate, (2) one of the highest peak and average brightness within the U.S., (3) a GeV-scale beam energy, (4) an extremely stable beam, (5) the availability of SRF and high-quality beams together, and, of course, (6) the IOTA storage ring capable of supporting a very broad range of ring-based advanced beam dynamics experiments. These unique features have a potential to foster a broad program in advanced accelerator R&D that cannot be explored at other facilities.

Besides these high priority tests, which are to be supported by Fermilab's Accelerator Science program, a number of studies can be performed by the broader user community at the IOTA ring and its injectors utilizing facility's unique beam

^{*} also Department of Physics and Northern Illinois Center for Accelerator & Detector Development (NICADD), Northern Illinois University, DeKalb IL 60115, USA

capabilities. The facility is foreseen to be able to serve a broad community intensity-frontier and energy-frontier-motivated researchers from many institutions (FNAL, CERN, ORNL, LBNL, JLab, NIU, CSU, University of Maryland, JINR/Dubna and BINP/Novosibirsk are already among the collaborating institutions). The ASTA team welcomes interested users without regard to national or institutional affiliation and researchers from national- and international universities and groups, the Department of Energy's National Laboratories; small business and industrial companies. ASTA users' meetings are held annually, the first two took place in July 2013 and in June 2014 [2].

1.1.2 Facility overview & capabilities

The construction of the ASTA facility is staged. The first stage enables a low-energy AARD program based on the photoinjector (~ 50 MeV) and a 300 MeV program based on a single SRF cryomodule, with associated beam transport lines and beam dumps; see Fig. 1.

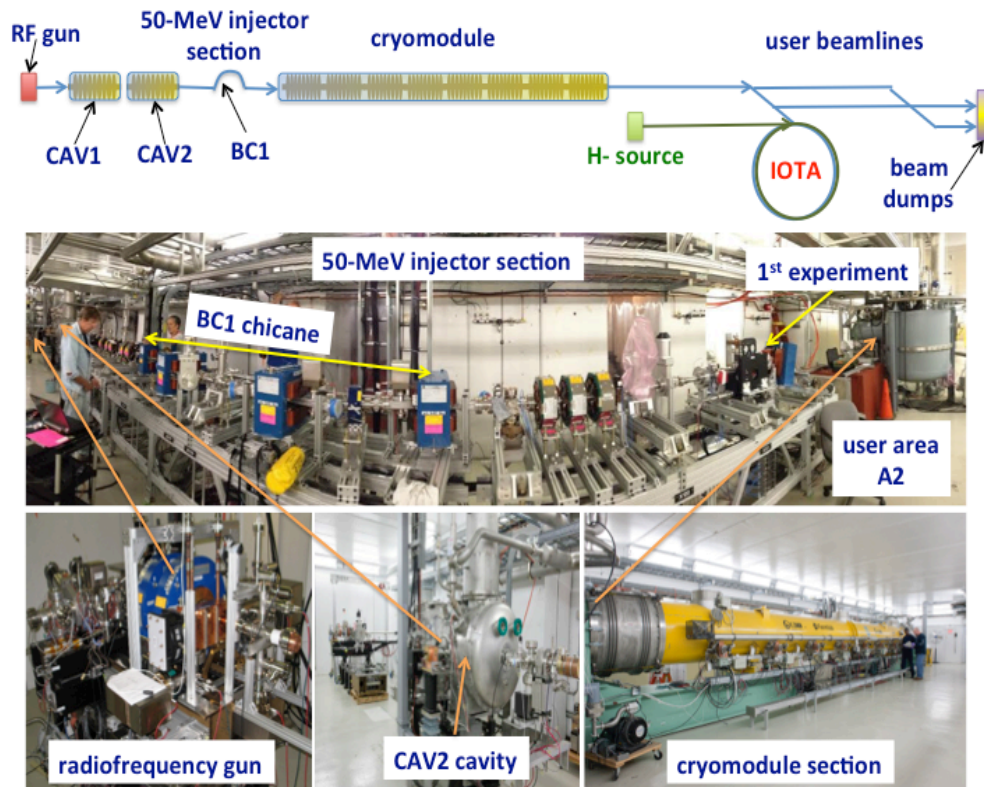


Figure 1: Overview of ASTA (**top row**) and photographs of the beamline sections (**middle and lower rows**). The labels “CAV1” and “CAV2” correspond to superconducting TESLA-type cavities, “BC1” is a magnetic-chicane bunch compressor, and “IOTA” stands for integrable-optics test accelerator. The total length of the facility is approximately 130 m.

The first stage also enables one of the transformative beam dynamics experiments: exploration of novel, non-linear accelerator lattices in the Integrable Optics Test

Accelerator (IOTA). An overview diagram of the foreseen facility in its first phase appears in Fig. 1 along with photographs of key subsystems already installed or in operation at the facility. Longer-term plans for expansion of ASTA are discussed at the end of this report.

Several experimental areas will be available to users for installation of experiments. A low-energy area situated within the photoinjector (eventually including an off-axis beamline), will provide electron bunches, possibly compressed, with energies up to ~ 50 MeV. A high-energy experimental area located downstream of the cryomodule section incorporates two (possibly three) parallel beamlines and the IOTA ring. Beam can in principle be delivered to the various user beamlines and IOTA quasi simultaneously as switching the beam from one beamline to the other would only require minor optical-lattice adjustment. Finally, the eventual availability of a H^- source would allow IOTA to be operated independently from the ASTA electron-beam users.

1.1.2.1 *Injector and superconducting radiofrequency (SRF) linac*

The backbone of the ASTA facility is a normal-conducting radiofrequency (RF) photoinjector coupled with 1.3-GHz superconducting accelerating cryomodules (CMs); see Fig. 1. The electron source consists of a 1-1/2 cell 1.3-GHz cylindrical-symmetric RF gun [3] comprised of a Cs_2Te photocathode illuminated by an ultraviolet (UV, $\lambda = 263.5$ nm) laser pulse. The photocathode drive laser is capable of producing a train of bunches repeated at 3-MHz within a 1-ms-duration macropulse [4]. The train are repeated at a 5-Hz frequency; see Fig. 2 (right). The laser system consists of a commercial fiber-based seed laser followed by a free-space chain of amplifiers; see Fig. 2 (left schematics). The seed laser was designed and built by Calmar Laser Inc.TM. It is an active mode-locked Yb-fiber system centered at $\lambda = 1054$ nm in the infrared (IR). The laser cavity consists of Yb-doped fiber amplifier, output coupler, electro-optics modulator, tunable filter, and fibers linking each component. A piezo stage is used to adjust the cavity length and achieve stable mode locking. The output-pulse duration is typically measured to be ~ 4 ps (rms). The laser is locked to a 1.3-GHz master oscillator. The modulator DC bias voltage requires constant adjustment to ensure proper mode locking as it typically drifts over time. This adjustment is typically made automatically through a feedback system. The output from the seed laser then passes through a pulse picker, which yields a ~ 1 -ms long train consisting of bunches repeated at a frequency 3 MHz. The pulses are then amplified by a chain of free-space single-pass amplifiers yielding a single-pulse energy of ~ 9 μJ . These amplifiers are based on end-pumped Nd:YLF crystals pumped with 100QCW or 200QCW diodes from Dilas Inc.TM. The final amplification is accomplished with a high-power amplifier pumped by Northrop-GrummanTM diodes and yield a pulse energy of ~ 180 μJ . Finally, the IR pulses are frequency converted to UV via two second-harmonic-generation stages before being transported to the accelerator vault in an evacuated transport line including a relay-imaging optics.

The 5-MeV electron bunches exiting the RF gun are then accelerated with two SRF TESLA-type cavities (CAV1 and CAV2) to approximately 50 MeV; see Fig. 1. Downstream of this accelerating section the beamline includes quadrupole and steering dipole magnets, along with a four-bend magnetic compression chicane (BC1) [5]. The beamline also incorporates a round-to-flat-beam transformer (RTFB) capable of

manipulating the beam to generate a high transverse-emittance ratio [6]. In the early stages of operation, the electron bunches will be compressed in BC1. In this scenario the longitudinal phase space is strongly distorted and the achievable peak current limited to less than 6 kA. Eventually, a longitudinal phase-space linearizer will be added thereby enabling the generation of bunches with 10-kA peak currents. An active linearizer, based on a 3.9-GHz cavity, and a passive linearizer, based on a high-impedance structure [7,8], are being considered as possible option for the linearizer structure. In addition the linearizer could also be used to tailor the current profile of the electron bunch [9,10]. The photoinjector was extensively simulated and optimized [11]. At a later phase the photoinjector will eventually include an off-axis experimental beamline branching off at the second dipole of BC1 in support to low-energy (<50-MeV) beam-physics experiments and diagnostics R&D.

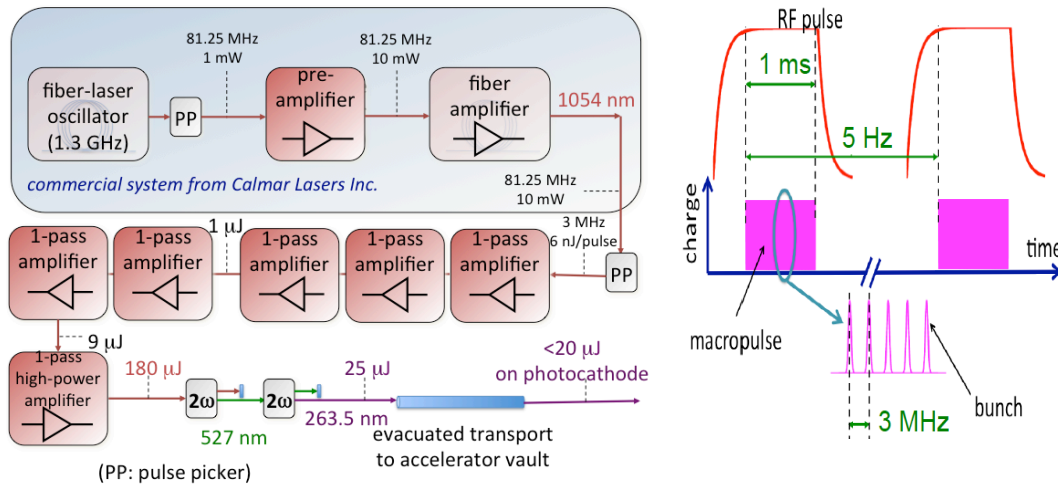


Figure 2: Block diagram of the photocathode drive-laser system (**left**) and schematics of the nominal beam temporal format (**right**). The macropulse format is adjustable within the range summarized in Table. 1

The 50-MeV beam is then injected into the SRF linac, which could eventually consist of three, 12-m long, TESLA/ILC-type CMs. Each CM includes eight 1.3-GHz nine-cell cavities. The first two CMs are foreseen to be of TESLA Type-III+ design, whereas the third (CM3) will be an ILC Type-IV design [12]. Together, these three CM's would constitute a complete ILC RF Unit. The SRF linac will be capable of providing an energy gain of ~750-MeV. The installation of the CM will be staged pending the completion of their construction.

Downstream of the linac is the high-energy test beam line section, which includes an array of multiple high-energy beam lines that transport the electron beam from the accelerating cryomodules to one of two beam dumps. The expected beam parameters are summarized in Table 1.

The beamline is instrumented with a comprehensive suite of diagnostics including electromagnetic beam position monitors, beam-current monitors, scintillating (Ce:YAG) at low energies and optical transition radiation (OTR) screens for

measurements of the beam's transverse density. A sub-ps resolution streak camera is also available along with other bunch-length diagnostics based on frequency analysis of the coherent THz radiation (either synchrotron or transition) produced by the electron bunch. Precise beam-arrival monitor based on electro-optical sampling are being developed.

Table 1: Anticipated electron-beam parameters for the ASTA linac. The ranges are values expected for lower/larger bunch charge. Higher peak current are realized to the detriment of transverse emittance. After bunch compression in BC1, the horizontal and vertical beam emittances are different.

<i>Parameter</i>	<i>Nominal value</i>	<i>Range</i>	<i>Unit</i>
Beam energy	300 (1 CM) 800 (3 CMs)	50-800	MeV
Bunch charge	3.2	0.02-20	nC
Bunch spacing	333	10- ∞	ns
Bunch train duration	1	0-1	ms
Train frequency	5	0.1-5	Hz
RMS normalized emittance	~ 5 (uncompressed)	$< 1, > 100$	μm
RMS bunch duration	1	0.01-10	ps
Peak current	5	0.05-10	kA

1.1.2.2 *Integrable-optics test accelerator (IOTA) ring*

ASTA layout includes a small storage ring to enable a ring-based AARD program in advanced beam dynamics of relevance to both Intensity and Energy Frontier accelerators. The Integrable Optics Test Accelerator (IOTA) ring is ~ 40 meters in circumference and will be capable of storing electrons from 50 to 150 MeV in energy [13]. Figure 3 shows the placement of the ring in the ASTA facility layout. It is planned to further expand capabilities for AARD in ASTA by installing of a 2.5-MeV proton/ H^- RFQ accelerator that was previously used for High Intensity Neutrino Source (HINS) research at Fermilab's Meson Detector Building facility [14].

The IOTA lattice is required to be periodic, with the element of periodicity comprised of a drift space with equal beta-functions, and a focusing and bending block with the betatron phase advance in both planes equal to π [a block dubbed " T -insert" in Figure 4 (a)]. The drift space must be long enough (> 2 m) to accommodate practical nonlinear magnets. The T -insert must be tunable to support a wide range of phase advances (and beta-functions) in the drift space in order to study different betatron tune working points. The focusing block is achromatic in order to avoid strong coupling between the transverse and longitudinal degrees of freedom. The ring must have one long (~ 5 m) straight section to accommodate a planned proof-of-principle experiment on optical stochastic cooling (OSC). Finally, IOTA has to fit within the footprint of the experimental hall and be properly oriented with respect to the injection line.

In its current design the ring is made of four cells. The cells are mirror-symmetric in pairs, and each consists of eight quadrupoles and two dipole magnets bending by 30 and 60 degrees. Given the betatron phase advance per cell of 0.8, a total betatron tune of 3.2 is achieved. Hence, in the extreme case the maximum tune shift generated by the nonlinear magnets may reach 1.6, leading some particles within the bunch to cross an integer resonance.

The IOTA-lattice design provides 2-m insertions for the nonlinear magnets, two 1-m-long straight sections for RF and other systems, and two 5-m sections – one for injection/extraction and another to accommodate a proof-of-principle experiment on optical stochastic cooling. Five quadrupole magnets are at least required to implement an axially symmetric lens in a straight section. The large number of quadrupoles used in the ring allow for a wide range of tuning for the betatron tune, which can be varied between 2.4 and 3.6, and dispersion and momentum compaction. Table 2 lists the main parameters of the IOTA ring when operated with an electron beam.

Table 2: Anticipated IOTA-ring parameters.

Parameter	Value	Unit
e^- beam nominal kinetic energy	150	MeV
e^- beam nominal intensity	1×10^9	e^-
e^- transverse rms emittance	0.1	μm
p^+ beam nominal kinetic energy	2.5	MeV
p^+ beam nominal intensity	8×10^{10}	p^+
p^+ transverse rms emittance	1-2	μm
Circumference	~ 40	m
Bending field	0.7	T
Beam pipe diameter	50	mm
Maximum beta function β_x, β_y	12, 5	m
Momentum compaction	[0.02 \div 0.1]	–
Betatron tune	[3 \div 5]	–
Natural chromaticity	[-10 \div -5]	–
e^- synchrotron radiation damping time	0.6	s
RF voltage, frequency, harm. Number	30, 30, 4	kV, MHz, –
e^- synchrotron tune	[0.002 \div 0.005]	–
e^- bunch length	[1 \div 2]	cm
e^- momentum spread	1.4×10^{-4}	–

Figure 3 depicts the proposed location of HINS within the ASTA facility. The HINS accelerator starts with a 50-kV, 40-mA proton (or H^- ion) source followed by a two-solenoid low energy beam transport (LEBT) line. The protons/ions are then accelerated by the pulsed 325-MHz RFQ to 2.5 MeV (with ~ 1 ms pulse duration) before injection into IOTA. The source will be located near the end of the electron beam line

and will incorporate a debunching cavity necessary to reduce the relative energy spread to below 10^{-3} . A bending magnet will steer the proton beam into the injection line to IOTA. The injection line is also used to inject electron beams from the ASTA linac in IOTA.

The IOTA ring will be equipped with 16 button-type beam-position monitors necessary to allow for a precise measurement of the betatron function in the drift upstream of the T -insert. In addition, optical windows located in the dipole-magnet vacuum chambers will permit extraction of synchrotron radiation for non-interceptive diagnostics. Finally, quadrupole pickups capable of non-interceptive measurement of the quadrupole moment of the transverse beam distribution are under consideration.

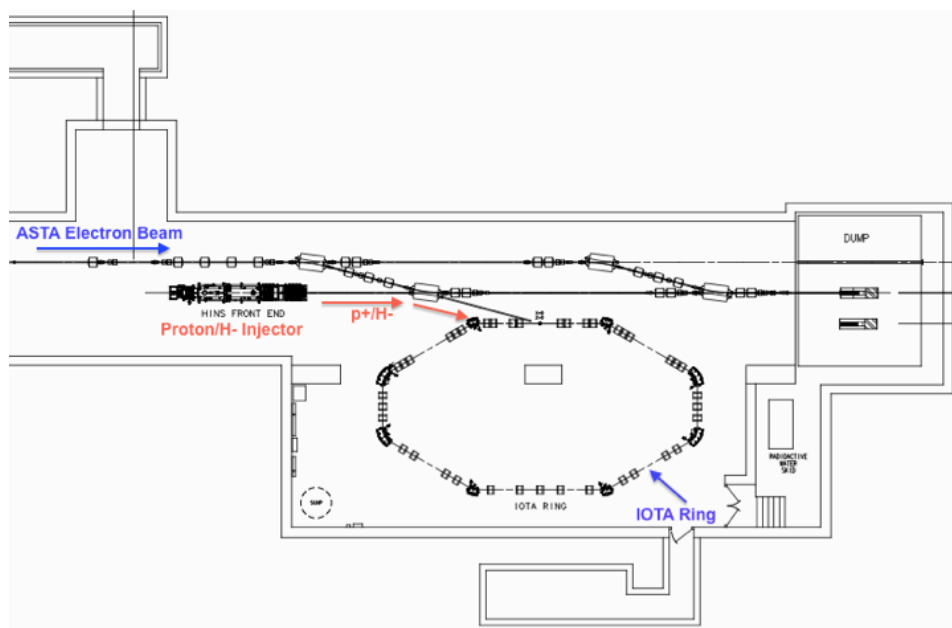


Figure 3: Layout of the IOTA ring within the ASTA facility.

1.1.2.3 *Superconducting radiofrequency (SRF) infrastructure*

The SRF infrastructure at ASTA was originally designed as an ILC test area in support of operating one ILC RF unit (a string of three cryomodules). It has since been repurposed to support the ASTA user facility. In this scheme, the main SRF devices are two single-cavity cryomodules dubbed cavity 1 and 2 (CAV1, CAV2 in Fig. 1) and one eight-cavity TESLA-style cryomodule. All of these systems are designed to operate with a 1.6-ms long pulse and a 5-Hz repetition rate. Regardless, the necessary RF, cryogenics, controls interlocks and diagnostics systems exist and have been made operational for this SRF facility. The main subsystems include (1) a cryogenics system capable of providing up to 120 Watts of 2K cooling, (2) a 5-MW klystron and associated high voltage supply and modulator for the 8-cavity cryomodule. A 10-MW multi-band klystron is on hand should more cryomodules be installed at ASTA, (3) two 300-kW klystrons and high-voltage sources for each of the two cavities (CAV1 and 2 in

Fig. 1), (4) low-level RF drive systems for each klystron/RF module, an adaptive Lorentz force detuning compensation system for each, (5) interlock systems for each unit, which can provide fast response/shut down in case of a fault, (6) digitized readouts of diagnostics, and (7) interface and user control via Fermilab's accelerator controls network (ACNET) [15]. Further details on these subsystems can be found in Ref. [16,17].

In Ref. [18] operation of the first SRF device to be installed at ASTA is described. CAV2 is a single cavity 9-cell device of TESLA design. Its original operation of CAV2 at ASTA was to provide a heat load for commissioning of the cryogenics system as well as to provide installation and operating experience with an SRF system prior to the arrival of the first ILC-style cryomodule. Since 2010 CAV2 has been operated in two periods with warm-up to room temperature necessary to accommodate cryomodules installation. A peak gradient of 24.5 MV/m has been achieved although recent operation has been limited to 21 MV/m due to coupler vacuum activity and excessive field-emission probe activity in the RF input coupler. An additional single cavity cryomodule, CAV1, is currently being upgraded with a higher-gradient cavity, tested to 29 MV/m at Fermilab's horizontal test stand. Installation is expected in late 2014. CM1 was the first 8-cavity ILC/TESLA-type cryomodule to be operated at ASTA. During its stay between 2010 and March 2012 it was cooled down and operated at 2K with its eight cavities achieving peak gradients between 20.2 and 28.2 MV/m. CM1 has since been removed. In April 2013 a second eight-cavity cryomodule, CM2 was installed at ASTA. CM2's history and performances to date are documented below. Reference [19] extensively summarizes SRF activities at ASTA to date.

1.1.3 Planned experiments & opportunities

The combination of a state-of-the-art superconducting linear accelerator and a flexible storage ring enables a broad research program directed at the particle physics accelerators of the future. Synopses of *some* of the enabled opportunities are discussed below.

1.1.3.1 IOTA-based experiments

The proposed research program includes at IOTA has expanded well beyond its initial goal to test non-linear, integrable, accelerator lattices, which have the potential to shift the paradigm of future circular accelerator design [20, 13]. IOTA will also enable the exploration of a range of topics supporting the high-intensity frontier. The electron beam is expected to enable a proof-of-principle experiment on optical-stochastic cooling [21]. The addition of a H^- source will also enable the investigation of integrable optics in presence of significant space charge effects. The H^- beam will also open the path to the study of space-charge compensation schemes in high-intensity circular accelerators [22]. IOTA will also support some fundamental Physics studies such as the measurement of the wave function associated to a single electron using a method similar to an experiment previously attempted [23].

1.1.3.1.1 Integrable-optics

Achieving high-intensity in circular accelerator is often limited by machine resonances, tune shifts and spreads, and collective instabilities. These three phenomena

are interdependent in all present accelerators, which employ a “linear” focusing optics. A path towards the potential mitigation of these limiting factors consists in designing accelerators that operates in a nonlinear beam-dynamics regime [24,25]. Practical implementations of such ideas proved elusive until recently when a solution for nonlinear integrable accelerator lattice that can be implemented with tailored magnets was discovered [20].

The ASTA facility will offer a unique opportunity to carry out the proposed research toward demonstration of the feasibility of the integrable optics technique. That research requires the construction and operation of a dedicated storage ring (IOTA) and cannot be carried out at the existing storage rings as it involves very special insertions (highly nonlinear magnets), which extend over a significant fraction of the ring circumference, special arrangements of the optics lattice and precise control of the elements (strength, positions, etc.).

In a first stage nonlinear magnets [see Fig. 4 (b)] will be used and the single-particle (nonlinear) dynamics of the ring will be investigated using pencil electron beams produced by the ASTA linac. Subsequently, the influence of space charge effects would be explored using H^- beams produced from the HINS source. Eventually, the inclusion of an electron lens formerly used for halo-collimation and tune-shift control in the Tevatron could also serve as a nonlinear element.

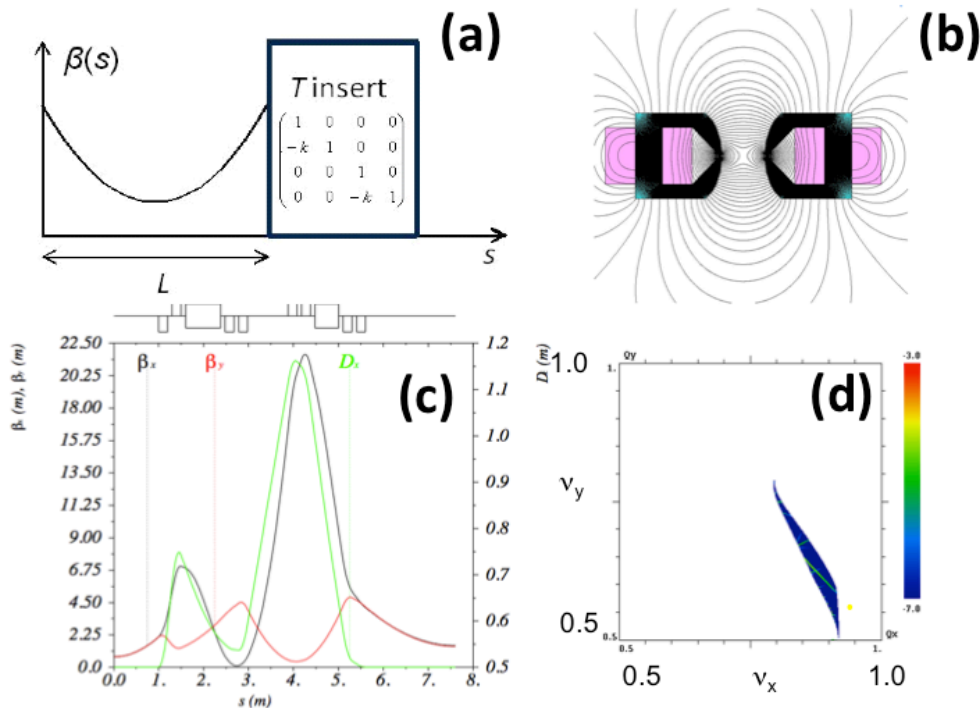


Figure 4: Configuration of one lattice cell: a drift space with equal beta-functions followed by a “ T -insert” (a), cross section of a nonlinear insert (b), betatron (red and black traces) and horizontal dispersion (green trace) functions over two lattice cells (c), example of fractional tune footprint obtained from frequency-map analysis (d).

1.1.3.1.2 Optical-stochastic cooling

Besides the experiments on highly non-linear integrable optics, the 150-MeV electron storage ring IOTA at ASTA will be used to carry out proof-of-principle experiment on optical stochastic cooling (OSC). The concept of OSC was proposed in the early 90's [26] and remains untested despite its significant advantage of allowing an increase of the stochastic-cooling bandwidth by ~ 3 to 4 orders of magnitude compared to microwave-based stochastic cooling. OSC therefore results in a significant decrease of damping time in high luminosity hadron colliders from thousands of hours to below an hour. Consequently, a successful demonstration of OSC would allow for effective luminosity control during a store and has potential serious implications for a range of heavier (than electron) particle accelerators, ranging from LHC and Muon Collider to other rings.

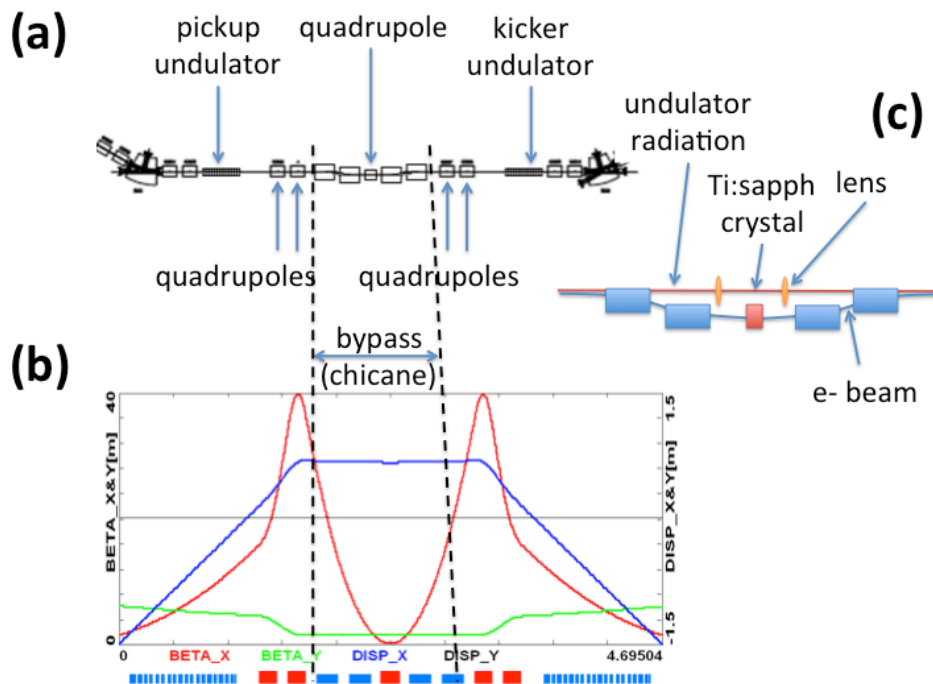


Figure 5: Configuration the optical-stochastic cooling in a 5-m long straight section of IOTA (a), associated design lattice functions (b), and close up of the bypass chicane showing the optical transport (red path) for the undulator radiation (c).

Figure adapted from Ref. [21].

The experiment will consist of two stages. In a first stage the cooling will be attempted without the inclusion of an optical amplifier: the radiation pulse produced by the pickup undulator will be directly refocus in the kicker undulator. Calculations indicate that undulator radiation without amplification should still provide a damping rate higher than the cooling rate due to synchrotron radiation. In the second stage, higher damping rates will be attempted by amplifying the pickup undulator-radiation pulse before coupling it back to the beam in the kicker undulator. One of the main

challenges is to achieve significant amplification within a short footprint to insure the optical pulse can still be overlapped in the kicker with the electron bunch slice that originated the radiation pulse in the pickup undulator. Another critical factor is the requirement for optical amplification with minimal distortion over the full spectrum of the radiation. These two requirements call for the design of a high-gain single-pass optical amplifier (OA). The OA will be based on a Titanium-Sapphire (Ti:sapph) medium capable of supporting amplification over large optical bandwidth and a prototype Ti:sapph laser is currently being developed at Fermilab.

The IOTA ring will offer unique opportunity to carry out the proposed research toward demonstration of the feasibility of the optical stochastic cooling technique. The 100-150 MeV electrons beam combined with ~ 6 -cm-period undulator will produce optical pulses with wavelength centered around 800 nm suitable for amplification with Ti:sapph. Figure 5 shows the configuration of the OSC in IOTA and the simulated lattice functions. The radiation from the pickup undulator will be focused on the Ti:sapph crystal and imaged back in the kicker undulator. Further details can be found in Ref. [21]. It should finally be pointed out that one of the capability to be demonstrated – the amplification of radiation fields produced by electron bunches – could have far-reaching applications well beyond OSC to, e.g., electron-beam diagnostics and manipulations or accelerator-based radiation sources.

1.1.3.1.3 Space-charge compensation for high-intensity circular accelerators

Through its past success in electron cooling of high-energy antiprotons [27], beam-beam compensation using electron lenses [28], and controlled halo removal by hollow electron beams [29], Fermilab has gained extensive experience and resources in manipulating high-energy particle beams by means of well-controlled electrons. As the mission of US high-energy physics program is pushing the Intensity Frontier, it is of great technical and scientific merit for the community if these techniques could be applied to overcome the beam intensity limit in the present accelerator technology. Consequently, IOTA is also foreseen to support investigation on novel methods of space-charge-compensation methods to achieve very intense and stable beams in circular accelerators through trapping and controlling of the electrons generated from beam-induced residual gas ionization. The method has a great potential to improve performance of leading high-current proton accelerator facilities and experiments, such as the Long-Baseline Neutrino Experiment (LBNE), Mu2e and $g-2$ after the intensity upgrades, and in compressor and accumulation rings envisioned in the Neutrino Factory and Muon Collider projects. The method may also offer a transformational technology for the next generation of high-intensity proton sources, e.g., such as those needed for the Accelerator Driven Systems.

The main idea of this compensation method is based on the long-known fact that the negative effect of Coulomb repulsion can be mitigated if beams are made to pass through a plasma column of opposite charge. This idea has been successfully applied to transport high-current low-energy proton and H^- beams into the RFQ in many linacs. In circular machines, partial neutralization by ionized electrons was attempted with notable improvements in beam intensity, namely one order of magnitude higher than the space-charge limit. However, the beam-plasma system was subject to strong transverse electron-proton ($e-p$) instability. In principle, this difficulty can be overcome if protons

and electrons are immersed in a longitudinal magnetic field which is a) strong enough to freeze the electron density distribution; b) strong enough to suppress the e-p instability; c) weak enough to allow positive ions to escape transversely, in addition to longitudinal draining; and d) uniform enough to avoid beta-beat excitations. In addition, we note that significant improvements have been made on the physics of non-neutral plasmas and on the stability of beam-plasma systems in the plasma physics community over the past decade, some of which could be readily adopted for the present project.

The existing components from the HINS program to be reused as an injector for the IOTA ring will facilitate researches on space-charge-compensation scheme. Additionally, the Tevatron electron lens system, a nonlinear element to be installed in IOTA ring, can be used to trap electrons for the initial space-charge compensation experiments. The experimental program will include the studies of the physics of electron column formation [30] and the stability of beam-plasma system, the measurements of electron accumulation and beam-plasma stability at HINS beamline, the design and construction of charge-exchange injection system for IOTA ring, and the measurements of electron accumulation and beam-plasma stability at IOTA ring using the electron lens system [22].

1.1.3.2 *Linac-based experiments*

1.1.3.2.1 Accelerator R&D at the Energy and Intensity Frontiers

The availability of advanced phase space manipulations (flat beam generation [6] and eventually transverse-to-longitudinal phase space exchanger [31]) will support the development and test of beam-driven acceleration methods, which would greatly benefit from shaped current profiles to significantly increase the transformer ratio - the energy gain of the accelerated bunch over the energy loss of the driving bunch. When combined with the aforementioned round-to-flat beam transformation, transverse-to-longitudinal exchanger could enable the production of electron bunch suitable for acceleration in asymmetric structures [32] or provide a tool for arbitrary emittance repartitioning within the three degrees of freedom. Other acceleration methods to be tested at ASTA include beam-driven acceleration in crystalline media [33].

Finally, the high-power beam produced by the SRF linac will provide opportunities for high-energy Physics detector R&D. These include the high-power tests of target required for the LBNE [34] and the generation of tagged-photon beams necessary to test components associated high-energy-physics detectors [35].

1.1.3.2.2 Accelerator R&D for Future SRF Accelerators

High gradient, high-power SRF systems are critical for many accelerator facilities under planning for the needs of high-energy physics, basic energy sciences and other applications. ASTA offers a unique opportunity to explore most critical issues related to the SRF technology and beam dynamics in SRF cryomodules. The low injection energy ~ 50 MeV combined with achievable low emittance beams is well suited to explore beam dynamics effects and especially beam degradation due to the time-dependent field asymmetries introduced by the input and higher-order mode (HOM) couplers. The pulsed operation of SRF cavities at high-gradient while accelerating mA beam currents over a long macropulse is also relevant to the International Linear

Collider (ILC) program. Furthermore, the SRF linac will provide an experimental platform necessary to develop the required low-level RF controls for the PiP-II pulsed linac [35]. Additionally, comprehensive beam-based measurements of long-range wakefield in SRF CMs are being planned using an upgraded version of the photocathode laser that would enable the production of charge-modulated bunch trains. Scanning the charge-modulation frequency and recording the HOM-induced beam displacements downstream of the cryomodule under test would enable the characterization of HOMs over a continuous range of frequencies [36]. Finally, a precise characterization of the jitter and beam-based stabilization of the SRF cryomodule has been proposed. It relies on the measurement of the bunch relative time of flight downstream of a bunch compressor, bunch energy and on the detection of coherent synchrotron radiation. These measurements are fed to an algorithm and used to control the phase and amplitude of the SRF cryomodules.

It was also pointed out that with appropriate changes in the RF system, the ILC-type cryomodule installed at ASTA could in principle be operated in CW mode and support tests relevant to the proposed next-generation CW light sources such as LCLS-II [37]. The cryogenic system and HOM couplers would limit the maximum gradient attainable by the cavities when operated in CW mode. Cryogenic considerations indicate that the maximum gradient would be limited to $\sim 5\text{-}7$ MV/m. Likewise, the ILC-type input coupler design nominally used at ASTA would limit the average beam current to <1 mA [38].

1.1.3.2.3 Accelerator R&D for Novel Radiation Sources

High energy, high-peak and high-average brightness electron beams are essential to the generation of high-brilliance high-flux light sources with photo energies ranging from keVs to MeVs. The high average power and brightness of the ASTA electron beam has unmatched potential for development of several novel radiation-source concepts.

Head-on collision of the electron bunch with an intense laser produces radiation with maximum upshifted frequency $\omega \simeq 4\gamma_L^2\omega_L$ where γ_L is the bunch's Lorentz factor and ω_L the laser frequency. At ASTA, colliding the bunch with a 800-nm laser would provide γ rays with energies ranging from ~ 1 to ~ 20 MeV; see typical spectrum in Fig 6 (left). If the laser repetition frequency matches the electron bunch frequency, an unprecedented γ -ray brilliance in excess of $\sim 10^{24}$ phot.mm⁻².mrad⁻².s⁻¹/(0.1%BW) could be attained [39]. The main technical challenge will be to develop a laser capable of producing Joule-level pulse energy with MHz repetition rate and will rely on a recirculating optical cavity [40]. Such high-flux γ -ray source is foreseen to be extremely beneficial to the measurement of the cross section associated to the $^{12}\text{C}(\alpha, \gamma)^{16}\text{O}$ reaction which is crucial in nuclear astrophysics as it enters in the synthesis of many elements. Due to its low cross section, a precise measurement of this reaction using a nucleation process in a bubble chamber remains elusive with presently available γ -ray sources (as only a handful of events per year are expected). The potential availability of a high-flux γ -ray source at ASTA could result in significantly higher statistics (up to 200,000 events per year) [41].

In the photoinjector area, it is foreseen to test a concept enabling the production of high-brilliance x rays by combining the low-emittance beam produced out of the photoinjector with channeling radiation (CR) [42,43]. The production of CR will occur downstream of the bunch compressor (BC1) [44]. Several crystal materials will be tested. Simulations using a 140- μm -thick diamond crystal indicate the production of x rays with energies in the [10-150]-keV range given the electron-beam energies available in the ASTA photoinjector (~ 15 to ~ 50 MeV); see Fig. 6 (right). The expected photon yield was estimated to $\sim 5 \times 10^8$ phot. $\text{mm}^{-2}.\text{mrad}^{-2}.\text{s}^{-1}/(0.1\% \text{BW})$ [43].

Additionally, it was suggested that the available long stable bunch train could serve for a proof-of-principle experiment of an extreme-ultraviolet (EUV) radiation source. An FEL oscillator operating at 13.4-nm wavelength was investigated and preliminary simulations indicate that saturation of the FEL process occurs after ~ 300 passes [42]. Initial experiments could be conducted at low energy (250-300 MeV) and provide 120-nm FEL radiation. An alternative configuration for the generation of EUV radiation consisting of a single-pass high-efficiency FEL is also being explored. FEL-based EUV sources driven by SRF linacs are expected to benefit to EUV lithography [43].

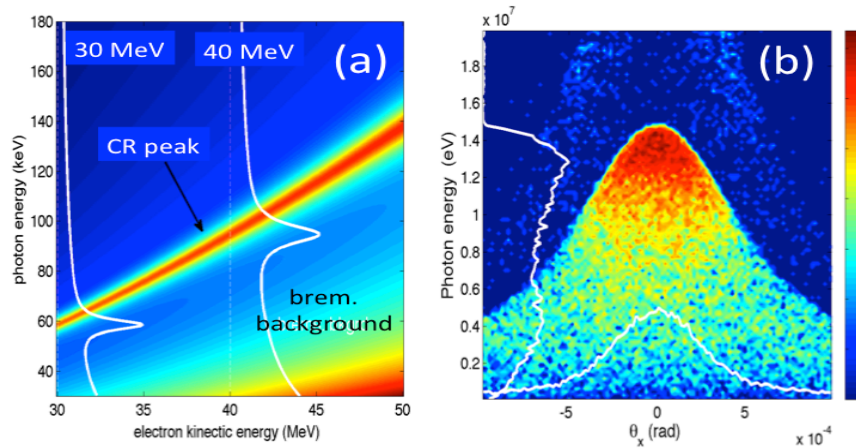


Figure 6: X rays spectral yield as function of electron beam energy (available in the ASTA photoinjector) and photon energy for the $1 \rightarrow 0$ transition along the (110) plane of diamond. Both CR and bremsstrahlung are considered in these calculations. The white traces are expected photon-energy spectrum for 30 and 40-MeV electrons (a). Spectral-angular distribution of γ rays produced by a 800-nm laser pulse backscattered on the ASTA 800-MeV beam (ultimately available with three cryomodules installed) (b).

Finally, the combination of flat beams with long bunch train could support the test of micro-undulators [47]. These micro-undulators, made of laser-micro-machined bulk rare-earth magnetic materials (SmCo and NdFeB), have magnetic fields with spatial period on the order of a few 100 μm . The associated undulator parameter is on the order of $K \sim \mathcal{O}(10^{-2})$ which results in a low photon yield $N \sim \alpha K^2$ (where α is the fine-structure constant). Therefore the test and characterization of the associated undulator radiation would greatly benefit from the long bunch train available at ASTA.

1.1.3.2.4 Accelerator R&D for Stewardship and Applications

With its high energy, high brightness, high repetition rate, and the capability of emittance manipulations built-in to the facility design, ASTA is an ideal platform for exploring novel accelerator techniques of interest for very broad scientific community beyond high-energy physics.

Some of the experiments include the development and test of subsystems and beam-manipulation schemes to improve the performance and decrease the cost of next-generation accelerator-based light sources. An example include the combination of the aforementioned phase-space manipulations to tailor the emittance partition within the three degrees of freedom to produce ultra-low emittance beams for future hard X-ray free-electron lasers.

Several low-cost ideas to “dechirp” the beam, i.e. to remove the residual correlated energy spread that generally subsists downstream of the final bunch compression stage in FEL drivers, were formulated and tested the past few years. The proposed dechirping methods include (i) the use of short-range wakefields impressed on the bunch as it passes in a dielectric [48] or corrugated [49] passive structure, or (ii) the judicious arrangement of three transverse-deflecting cavities to produce a transfer matrix with a non-vanishing longitudinal dispersion R_{56} [50]. In addition using these passive structures to further control the longitudinal-phase-space nonlinearities could also be tested at ASTA [51]. Demonstrating the compatibility of these techniques with high-repetition rate beam available at ASTA could lead to their inclusions in planned accelerator-based light sources drive by SRF linacs.

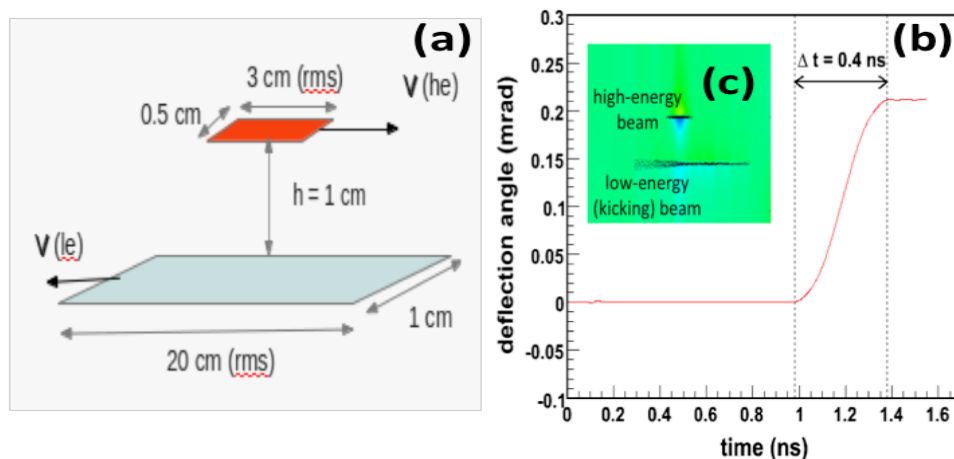


Figure 7: Overview of the beam-beam kicker configuration (a): A low-energy (“le”) high-charge beam is counter propagated to the high-energy (“he”) beam being kicked. Particle-in-cell simulations of a flat-beam kicker showing a rise time of ~ 400 ps (b). The inset (c) shows a side view (z, x) of the beam distributions (shown as dark dots) and associated (velocity) field E_x (appearing as a contour plot) [Courtesy of D. Mihalcea, Northern Illinois University].

The flat-beam transformation available at ASTA could also support tests relevant to nuclear-physics accelerator R&D, e.g., to validate the concept of a fast beam-beam kicker [52] or investigate beam dynamics challenges associated to the transport and manipulation of magnetized beams [53]. Preliminary simulations using ASTA beam

parameters with a 1-MeV 5-nC kicker beam indicate that rise time of ~ 400 ps could be achieved with kick strength in excess of ~ 20 mrad as depicted in Fig. 7. These researches could have important implications on, e.g., the Medium-energy Electron-Ion Collider (MEIC) [54] being explored at Jefferson Laboratory.

Finally, the beam available at ASTA will foster the development and tests of advanced beam diagnostics relevant to, e.g., CW FELs or energy-recovery linacs. Some of these diagnostics especially those capable of measuring single-bunch parameters within the RF macropulse, will be crucial for optimizing the feedback system needed to stably operate the ASTA SRF cryomodule(s).

1.1.4 Commissioning status

Commissioning of the subsystems comprising ASTA has been ongoing since 2010 in parallel with installation and construction activities. Similarly commissioning of these components has also been largely in parallel. In the coming months it is expected that bringing them into operation as an accelerator will be realized. Electrons with energies up to 50-MeV are foreseen in 2014. This will be achieved by operation of the RF gun at 5 MeV and two single-cavity cryomodules (CAV1 and CAV2) each capable of boosting the beam energy by 25 MeV. Beam will be delivered to a low energy absorber at the end of the injector section. Activities relating to these main components – laser, gun, beamline, and SRF components – are described below.

1.1.4.1 *Photocathode laser system*

Construction of the laser room at the ASTA facility in NML was completed in August 2012 and the commissioning of laser system was completed at the end of CY2012. The final UV bunch energy ranges from 0.1 to 3 μJ and the corresponding laser-pulse duration is approximately 3.8 ps (rms). Figure 8 provides snapshots of the evolution of a 100-pulse train throughout the IR amplifying chain, and downstream of the first (green) and second (UV) stages of the fourth-harmonic generation conversion. The pulse-intensity fluctuations within the bunch are maintained to less 5% throughout the laser system as shown in Fig. 8 (lower-right histogram).

In its present design, the photocathode laser system support a maximal bunch frequency of 3 MHz within a train. A next stage upgrade plan is to improve the operation of laser system. This limitation to 3 MHz came from a multi-pass amplifier that was recently substituted by three single-pass amplifiers. There is therefore no technical limitation toward increasing the intra-train operation frequency from 3 to 81.25 MHz. Although such a frequency increase would come at the expense of single-pulse energy (i.e. single bunch charge), it would extend the range of bunch-train format available to users and could, for instance, support experiments on higher-order mode investigation using charge-modulated bunch trains [36] or permit the generation of high-brilliance x-ray radiation via inverse Compton scattering.

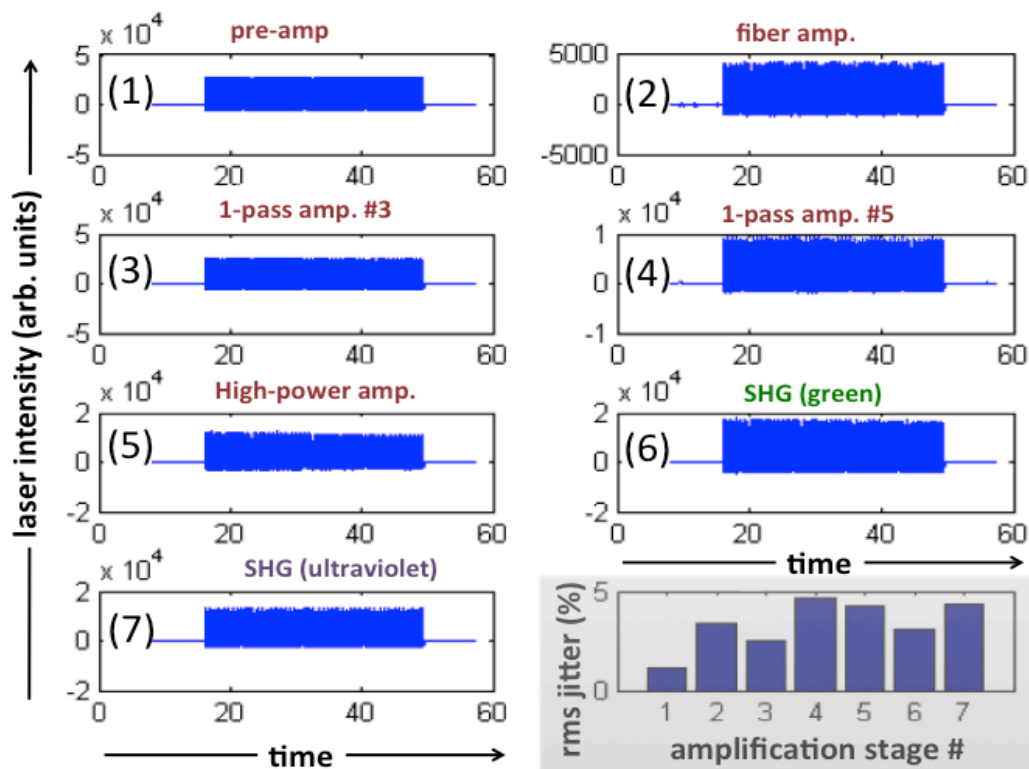


Figure 8: A single capture of 100 bunches on the VME-based digitizer from each of seven photodiodes installed throughout the laser system shown in Fig. 2 (left). The lower-right histogram provides the laser intensity fluctuation downstream of the amplification-stage number (corresponding to the numeric labels on the other plots)

1.1.4.2 *Radiofrequency gun characterization*

The gun system consists of three parts: gun-cavity, coaxial coupler with a “doorknob” transition and RF vacuum window. In 2011, the rf vacuum window (manufactured by Thales™) was first conditioned to ~ 4 MW [in two modes: fully reflected mode (20- μ s pulse length) and fully transmitted mode (1-ms pulse length)]. The power was limited by the klystron and arcing in an isolator. The conditioning of the assembled RF-gun system started in December 2012, and was completed in the middle of CY2013 given the limited availability of klystron(s) and on-going installation activities. The RF gun system was first conditioned up to 1.2 MW (1-ms pulse width, 5-Hz repetition rate) with a molybdenum cathode using a 4-MW klystron designated for cryomodule test. It was subsequently conditioned to 3.7 - 4.1 MW (1-ms pulse width, 1-Hz repetition rate) with a molybdenum cathode using a new klystron dedicated to the gun system. Finally, the molybdenum cathode was replaced with Cs₂Te-coated cathode and the system was reconditioned up to 3.7 - 4.1 MW (1-ms pulse width, 1-Hz repetition rate). This power level exceeded the required 3.5-MW power for a peak accelerating field of 45 MV/m at the cathode surface. During conditioning, the resonant frequency of the RF gun was controlled via the cooling-water temperature. However the water temperature response time is intrinsically slow and the control system is designed

for normal operation (stable power level). At higher average power levels (longer pulse width) a power change (either planned or unplanned due to events such as sparking) can cause rapid change of resonant frequency of the cavity, which would be out of our water-cooling control. To circumvent this issue, the klystron's operating frequency was manually adjusted to follow each sudden change of the cavity's resonant frequency.

ASTA successfully produced its first photoelectron beam from the gun to a Faraday cup on June 20th, 2013. The initial beam was produced using the bare molybdenum cathode, about 8-15 laser pulses at 1-Hz and electrons were observed on three of the primary diagnostics immediately downstream of the gun: loss monitor, resistive wall current monitor, and Cerium-doped yttrium aluminum garnet (Ce:YAG) screen. Due to the limited quantum efficiency of the bare-molybdenum photocathode the charge produced was very low (\sim pC). Subsequently a Cs₂Te-coated cathode was inserted into the gun in March 2014 and enabled the formation of 4-nC bunches downstream of the RF gun. After extensive conditioning of the RF gun and optimization of the laser system 1-ms bunch train were generated and measure with the Faraday cup; see Fig. 9. The pulse train is strikingly flat except for some transient fluctuations at the beginning of the pulse.

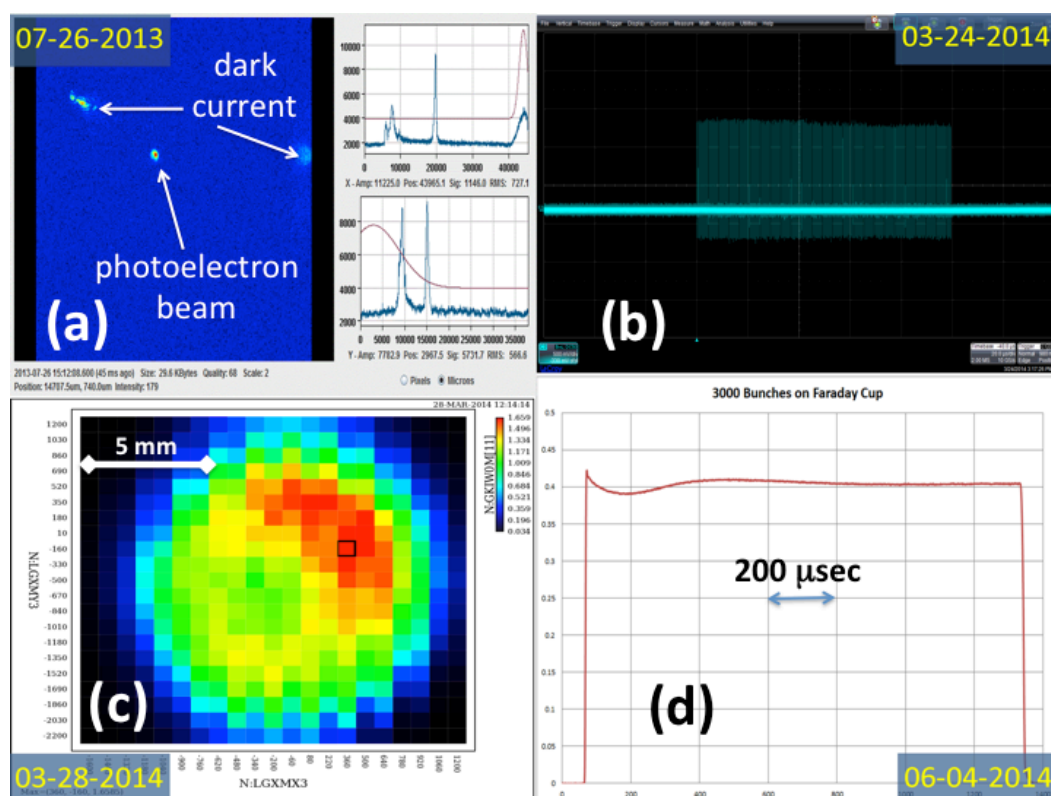


Figure 9: Milestone pertaining to the gun commissioning: first electron image on the Ce:YAG screen located downstream of the gun (a), first electron-bunch train produced with Cs₂Te cathode (b), quantum-efficiency map of the Cs₂Te cathode (c), and demonstrating of the production of 1-ms bunch train with 3000 pulses (d).

1.1.4.3 *Electron beam measurements*

The first characterization of the electron beam properties included beam intensity, beam energy, a beam-based calibration of the RF gradient, and emittance measurements at low charge. Preliminary results were presented in Ref. [55].

Measurements were based on the instrumentation available between the RF gun and the diagnostic table, placed about 1.1-m downstream of the photocathode. The main components were the bucking and main solenoids surrounding the gun cavity, horizontal and vertical trim dipole magnets, a Ce:YAG screen, and a Faraday cup. The maximum bunch intensity achieved is ~ 3 nC for a laser pulse energy of approximately 2 μ J, corresponding to a quantum efficiency of the cathode of 1.5%. The laser spot on the cathode was aligned with the electrical axis of the cavity by turning off the solenoids and by observing the displacement of the beam spot on the Ce:YAG screen as the phase of the RF gun was changed [56]. With this method, the accuracy of the laser-cavity alignment was about 0.1 mm.

A direct calibration of the beam energy, accurate to about 10%, was obtained by observing the deflection of the focused beam on the YAG screen as a function of the horizontal or vertical trim dipole settings. The RF gun power and phase were typically set to achieve a kinetic energy of 4.5 MeV.

Several properties of the RF gun and of the electron beam could be inferred from solenoid scans at low charge (less than 2 pC/bunch) with the nominal laser-pulse duration. The beam spot at the Ce:YAG screen was measured as a function of the solenoid settings. The main and bucking solenoids were kept at a fixed field ratio so that the magnetic field at the cathode was negligible. Under these conditions, transport between the cathode and the screen was emittance dominated. Therefore the beam dynamics could be modeled by transfer matrices that include the effects of cavity fields with superimposed solenoids. To evaluate systematic uncertainties, these transfer matrices were calculated with two models: the ASTRA tracking code [57] and a longitudinal slicing of the gun [58,59]. The peak field in the RF cavity, its phase, and the initial beam emittance were independent free parameters and they were inferred from a least-squares fit of the models to the data.

The peak fields had a statistical uncertainty of less than 1% and provided a beam-based calibration of the RF gradient. This method, based on gun and solenoid field maps, also provided a calibration of the final electron energy (derived from gradient and phase) independent from the direct deflection measurement with the trim dipoles.

Emittance values at low charge were in agreement with the expected intrinsic emittance of cesium telluride cathodes. For instance, for a typical rms laser spot size of 0.6 mm, we measured an rms-normalized emittance of 0.6 μ m. The drift of the beam spot on the screen as a function of solenoid current will be used to check the alignment of the magnetic axis of the solenoid. The space-charge model of the injector will be verified with solenoid scans at high charge (up to 3 nC/bunch).

In the coming weeks, we plan to accelerate electrons up to 20 MeV with CAV2 (see Fig. 1). The 20-MeV beam will enable the commissioning of the beamline connecting the photoinjector to the cryomodule as far as the low-energy beam absorber located upstream of the cryomodule.

1.1.4.4 *SRF cavities achieve ILC specifications*

Upon arrival in ASTA in April 2013 and after cool down to 2 Kelvin (23 Torr) in November 2013, cryomodule 2 (CM2) individual cavity characterization was carried out with seven of the eight cavities achieving a peak gradient of 31.5 MV/m as shown in Fig. 10 (left). The outlier was limited to 30.5 MV/m by quenching. The 31.5-MV/m gradient is an administrative limit consistent with the ILC gradient specification. Reference [60] describes the performance of the cavities prior to assembly into a complete module. The steps required to fully characterize each cavity: on-resonance coupler conditioning, tuning to resonance, signal calibration, peak gradient determination, measurement of dark current and X-ray field emission, and dynamic heat load (DHL) measurement to determine the Q_0 required on average one week to complete. Reference [61] describes early performance results. In recent weeks CM2 operation as a unit has been initiated: all cavities powered simultaneously, except cavity #8 which has a warm-coupler vacuum issue. This issue will be addressed in the future when an opportunity to warm the cryomodule to room temperature avails itself. Transitioning to the mode of unit powering required the installation of a waveguide distribution system fabricated by SLAC to allow the output of a single RF source (klystron) to power all cavities simultaneously. Variable tap offs to each of four pairs of cavities were adjusted to control what fraction of the total RF output is provided to each cavity pair. As of this writing the average accelerating gradient achieved per cavity is 30 MV/m with the system operating at the nominal pulse width of 1.6 milliseconds and 5-Hz repetition rate; see Fig. 10 (right). Adaptive Lorentz-force detuning compensation (LDFC) was active in order to maintain a relatively flat peak field within the macropulse.

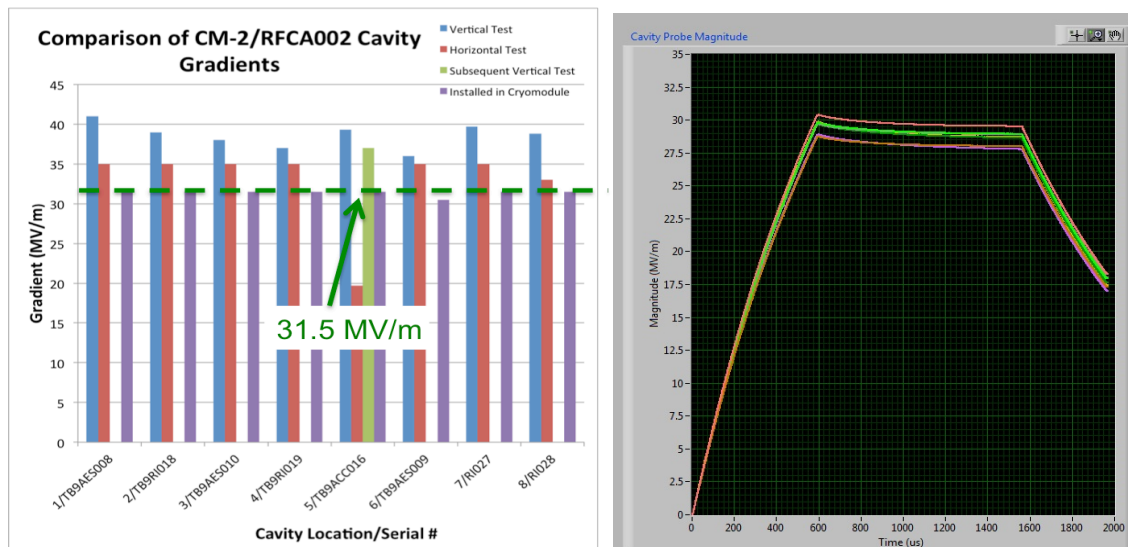


Figure 10: Comparison of CM-2/RFCA002 cavity gradients: vertical test (blue), horizontal (red), and in CM-2 (purple). An administrative limit of 31.5 MV/m was set for CM-2 testing (left). CM2 peak gradients achieved as of August 2014 in operation as a unit (right). The goal is operate all cavities within the cryomodule to at least 31.5 MV/m simultaneously.

A full suite of testing including raising the gradient to at least 31.5 MV/m, operating the low level RF system in closed loop, optimizing adaptive LFDC, and repeating DHL to measure the cumulative Q_0 will follow shortly. Plans call to operate CM2 with beam by end of CY2015.

1.1.5 Upgrade path

ASTA will evolve over time to address the demands of the accelerator R&D program. In its first stage the main subsystems of ASTA include a 50-MeV photoinjector source with auxiliary lasers systems, a linear accelerator based on a single SRF cryomodule, an electron-storage ring (IOTA) and several experimental areas for research with low-energy and high-energy beams. Possibilities exist to further expand the capabilities of the R&D program including the installation of a H^- source to expand the IOTA program to protons and the addition of SRF cryomodes to increase the linac beam energy. Depending on user demand, a staged bunch-compression system could also be incorporated and would rely on the addition of a linearizing cavity (a 3.9-GHz SRF cavity located downstream of CAV2).

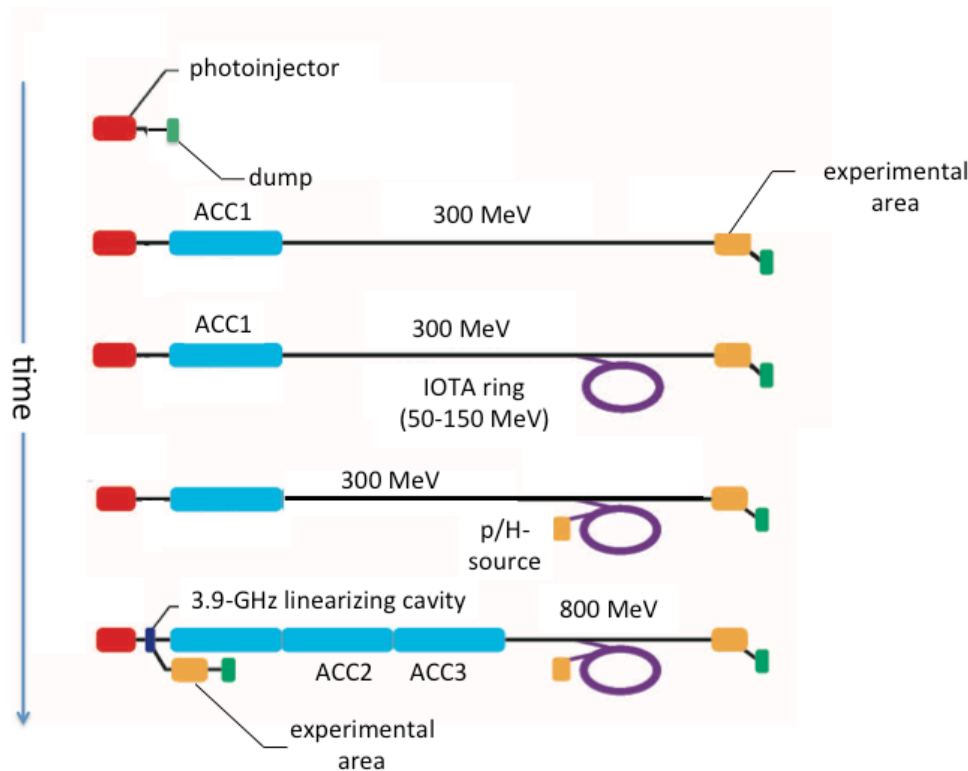


Figure 11: A possible path for staged construction of ASTA. Currently only the configurations shown in the top four rows are being pursued. Subsequent upgrade stage(s) will be guided by user demands.

We therefore envision a multi-staged approach to ASTA completion as illustrated in Fig. 11. The first stage enables a low-energy AARD program based on the photoinjector and a 300 MeV program based on a single superconducting cryomodule, with associated beam transport lines and beam dumps. The first stage also enables one of the

transformative beam dynamics experiments: exploration of novel, non-linear accelerator lattices in the Integrable Optics Test Accelerator (IOTA). The subsequent stages will ultimately be guided by user demands.

1.1.6 Acknowledgements

The ASTA scientific program was developed in partnership with many national laboratories, Universities, and companies; see list in Ref. [1]. The successful initial commissioning of ASTA would not have been possible without a team of dedicated scientific and technical staffs.

Fermilab is operated by Fermi Research Alliance, LLC under Contract No. DE-AC02-07CH11359 with the United States Department of Energy.

1.1.7 References

1. P. H. Garbincius, S. Henderson, J. Leibfritz, P. Piot, V. Shiltsev (Editors), "Proposal for an Accelerator R&D User Facility at Fermilab's Advanced Superconducting Test Accelerator (ASTA)," Fermilab TM-2568 (2013).
2. Information on ASTA can be found at <http://asta.fnal.gov>
3. B. Dwersteg, et al., "RF gun design for the TESLA VUV Free Electron Laser," Nucl. Instr. Meth. A **393**, 93 (1997).
4. J. Ruan, et al., "Commission of the Drive Laser System for Advanced Superconducting Test Accelerator," in Proc. of IPAC13, p. 3061 (2013).
5. C. R. Prokop, et al., "Beam dynamics performances and applications of a low-energy electron-beam magnetic bunch compressor," Nucl. Instr. Meth. A **719**, p. 17 (2013).
6. J. Zhu, et al., "Formation of compressed electron beams with high transverse-emittance ratio," Phys. Rev. ST Accel. Beams **17**, 084401 (2014).
7. P. Craievich, "Passive longitudinal phase space linearizer," Phys. Rev. ST Accel. Beams **13**, 034401 (2010).
8. M. Venturini, "Passive linearizer," presented at the 2nd Advanced Superconducting Test Accelerator Users Meeting, Fermilab, June 9-10, 2014, <https://indico.fnal.gov/event/8409>
9. P. Piot, et al., "Generation and characterization of electron bunches with ramped current profiles in a dual-frequency superconducting linear accelerator," Phys. Rev. Lett. **108**, 034801 (2012).
10. F. Lemery and P. Piot, "Ballistic bunching of photo-injected electron bunches with dielectric-lined waveguides," preprint arXiv:1407.1005 [physics.acc-ph] (2014).
11. P. Piot, et al., "Beam dynamics simulations of the NML photoinjector at Fermilab," Proc. of IPAC10, Kyoto, Japan, p. 4316 (2010).
12. T. Arkan, et al., "Superconducting RF cryomodule production & testing at Fermilab," Proc. of Linac10, Tsukuba, Japan, p. 599 (2010).
13. S. Nagaitsev, "Design and Simulation of IOTA - a Novel Concept of Integrable Optics Test Accelerator," Proc. of IPAC12, New Orleans, LA, p. 16 (2012).
14. R. C. Webber, et al., "Overview of the high-intensity neutrino source linac

- R&D at Fermilab,” Proc. LINAC08, Victoria, BC, 36 (2008).
15. ACNET user guide is available at <http://www-ppd.fnal.gov/ftbf/acnet.html>.
 16. E. Harms, et al, “Test Results of Tesla-style Cryomodules at Fermilab,” MOPB054, Proc. of LINAC2012, Tel Aviv, p 297 (2012).
 17. W. Schappert and Y. Pischalnikov, “Adaptive Compensation for Lorentz Force Detuning in Superconducting RF Cavities,” Proc. of SRF2011, Chicago, p 940 (2011).
 18. E. Harms, et al, “Operating Experience with CC2 at Fermilab’s SRF Beam Test Facility,” Proc. of LINAC2010, Tsukuba, p. 818 (2010).
 19. E. Harms, et al, “SRF Systems for ASTA at Fermilab,” Proc. of IPAC2014, Dresden, p. 2601 (2014).
 20. V. Danilov, S. Nagaitsev, “Nonlinear accelerator lattices with one and two analytic invariants,” Phys. Rev. ST Accel. Beams **13**, 084002 (2010).
 21. V. Lebedev, et al., “Test of Optical Stochastic Cooling in the IOTA Ring,” Proc. of NAPAC13, p. 422 (2013).
 22. M. Chung, et al., “Space-charge Compensation for High-intensity Linear and Circular Accelerators at Fermilab,” Proc. of NAPAC13, Pasadena, CA, p. 402 (2013).
 23. V.V. Danilov, et al., “Possible Experiments on Wave Function Localization Due to Compton Scattering,” Proc. of NAPAC13, Pasadena, CA, p. 919 (2013).
 24. E. M. McMillan, in Topics in Modern Physics. A Tribute to E. U. Condon, edited by E. Britton and H. Odabasi (Colorado University Press, Boulder, 1971), p. 219.
 25. V. V. Vechev and Yu. F. Orlov, “Fundamental properties of non-linear focusing,” J. Nucl. Energy, Part C Plasma Phys. **8**, 717 (1966).
 26. A. A. Mikhailichenko, M. S. Zolotarev, “Optical Stochastic Cooling,” Phys. Rev. Lett. **71**, 4146 (1993).
 27. S. Nagaistsev et al., “Experimental demonstration of relativistic electron cooling,” Phys. Rev. Lett. **96**, 044801 (2006).
 28. V. Shiltsev et al., “Experimental demonstration of compensation of beam-beam effects by electron lenses,” Phys. Rev. Lett. **99**, 244801 (2007).
 29. G. Stancari et al., “Collimation with Hollow Electron Beams,” Phys. Rev. Lett. **107**, 084802 (2011).
 30. V. D. Shiltsev, “New possibilities for beam-beam and space-charge compensation: MCP gun and electron columns,” in Proc. of PAC2007, p. 1159 (2007).
 31. P. Piot, et al. “Generation of relativistic electron bunches with arbitrary current distribution via transverse-to-longitudinal phase space exchange,” Phys. Rev. ST Accel. Beams **14**, 022801 (2011).
 32. D. Mihalcea, et al., “Three-Dimensional Analysis of Wakefields Generated by Flat Electron Beams in Planar Dielectric-Loaded Structures,” Phys. Rev. ST Accel. Beams **15**, 081304 (2012).
 33. Y.-M. Shin, et al., “Ultra-high gradient beam-driven channeling acceleration in hollow crystalline media,” in Proc. of IPAC14, Dresden, Germany, p. 1512 (2014).
 34. RaDIATE (Radiation Damage in Accelerator Target Environments) Collaboration, <http://www-radiate.fnal.gov/index.html>.

35. S. Henderson, S. Holmes, A. Kronfeld, R. Tschirhart, (Editors) "Project X: Accelerator Reference Design, Physics Opportunities, Broader Impacts," FERMILAB-TM-2557 (2013).
36. S. Fartoukh, "A new method to detect the high impedance dipole modes of TESLA cavities," report CEA/DAPNIA/SEA-98-18, Saclay, France (1998).
37. J. Galayda, "The Linac Coherent Light Source-II Project," Proc. of IPAC2014, Dresden, Germany, p. 935 (2014).
38. N. Solyak (Fermilab), private communication (2013).
39. A. Murokh (Radiabeam LLC), private communication (2013).
40. R. Tikhoplav, et al., "High-power pulse recirculation in a stable pseudo-confocal geometry," Opt. Lett. **37**, 4717 (2012).
41. C. Ugalde, et al., "First determination of an astrophysical cross section with a bubble chamber," Phys.Lett. B **719**, 74 (2013).
42. C. A. Brau, et al., "Channeling radiation as a source of hard x-rays with high spectral brilliance," Sync. Rad. News **25** (1), 20 (2012).
43. T. Sen, et al., "Spectral Brilliance of Channeling Radiation at the ASTA photoinjector," preprint arXiv:1407.6053v1 [physics.acc-ph] (2014).
44. B. Blomberg, et al., "Channeling radiation with low-energy electron beams: experimental plans & status at Fermilab," Proc. of FEL13, New-York NY, p. 38 (2013).
45. A. Lumpkin, et al., "Feasibility of an XUV FEL Oscillator at ASTA," Proc. of FEL13, New-York NY, p. 88 (2013).
46. A. Murokh and A. Tremaine (Organizers), "Collaboration meeting on FEL sources for EUV lithography: part II", Santa Monica, CA, April 23-24, 2014.
47. B. A. Peterson, et al., "Technology Development for Short-period Magnetic Undulators," Physics Procedia, **52**, 36 (2014).
48. S. Antipov, et al., "Experimental demonstration of energy-chirp compensation by a tunable dielectric-based structure," Phys Rev Lett. **112**, 114801 (2014).
49. P. Emma, et al., "Experimental demonstration of energy-chirp control in relativistic electron bunches using a corrugated pipe," Phys Rev Lett. **112**, 034801 (2014).
50. N. Yampolsky, et al., "Imposing Strong Energy Slews with Transverse Deflecting Cavities," talk at NAPAC13, Pasadena, CA, 2013 (unpublished).
51. P. Craievich, "Passive longitudinal phase space linearizer," Phys. Rev. ST Accel. Beams **13**, 034401 (2010).
52. V. Shiltsev, "Beam-beam kicker for superfast bunch handling," Nucl. Instr. Meth. Sec. A **374**, 137 (1996).
53. P. Piot, Y.-E Sun, "Generation and dynamics of magnetized electron beams for high-energy electron cooling," to appear in Proc. of the 2014 workshop on electron-ion collider, Newport News, VA, March 21-24, 2014 (in press).
54. S. Abeyratne, et al. [MEIC collaboration], "Science Requirements and Conceptual Design for a Polarized Medium Energy Electron-Ion Collider at Jefferson Lab," arXiv:1209.0757 [physics.acc-ph] (2012).
55. J. Ruan et al., "Commissioning status of the Advanced Superconducting Test Accelerator at Fermilab," Proc. of IPAC2014, Dresden, Germany, p. 2615 (2014).
56. F. Stephan et al., "Detailed characterization of electron sources yielding first

- demonstration of European X-ray Free-Electron Laser beam quality,” Phys. Rev. ST Accel. Beams **13**, 020704 (2010).
57. K. Flöttmann, “ASTRA: A Space Charge Tracking Algorithm,” <http://www.desy.de/~mpyflo> (April 2014).
 58. C. Gulliford and I. Bazarov, “New method for generating linear transfer matrices through combined RF and solenoid fields,” Phys. Rev. ST Accel. Beams **15**, 024002 (2012).
 59. G. Stancari, “Electron beam measurements in the ASTA rf gun,” presented at the 2nd Advanced Superconducting Test Accelerator Users Meeting, Fermilab, June 9-10, 2014, <https://indico.fnal.gov/event/8409>.
 60. A. Hocker, et al, “Individual RF Test Results of the Cavities Used in the First US-built ILC-type Cryomodule,” Proc. of IPAC2012, New Orleans, p 2321, (2012).
 61. A. Hocker, et al, “Results from RF Tests of the First US-built High-gradient Superconducting Cryomodule,” Proc. of IPAC2014, Dresden, p 2598 (2014).